**Journal of Contemporary Technology and Applied Engineering (JCTAE)**

**Home Page:** https://jctae.journals.ekb.eg/

**Published by:** Faculty of Engineering, Kafrelsheikh University

**Volume:** 3 **Issue:** 2 **Year:** 2025 **Pages:** 1 – 12

**DOI:** 10.21608/jctae.2024.306311.1033

**Print ISSN:** 2812-5797

**Online ISSN:** 2812-5800

# OPTIMIZING TRAVEL SPEED FOR MINIMIZING POROSITY AND ENHANCING MICROHARDNESS IN WAAM-DEPOSITED ER70S-6 STEEL

Received: 22-07-2024
Accepted: 06-08-2024

Mohammed Dekis[a,*], Mahmoud Tawfik[a], Mohamed Egiza[a], Montasser Dewidar[a]

[a] *Mechanical Engineering Department, Faculty of Engineering, Kafrelsheikh University, Kafrelsheikh 33516, Egypt,*

[*] Corresponding author: M. Dekis (mohamed_hashem@eng.kfs.edu.eg)

**ABSTRACT.** Optimizing process parameters in Wire Arc Additive Manufacturing (WAAM) is essential for high-quality, cost-effective ER70S-6 steel components. This study investigated the impact of travel speed (TS) on porosity and microhardness. Inappropriate parameter selection led to defects like discontinuous beads and irregular layers. Importantly, lower TS (120 mm/min) resulted in significantly higher porosity (15.58%) due to increased heat input and trapped hydrogen. Conversely, higher TS (180 mm/min) yielded a substantial reduction in porosity (2.04%), highlighting its role in controlling pore formation. Microhardness exhibited a complex relationship with TS and location, with faster cooling in bottom and top regions leading to higher values (216 HV). Additionally, increasing TS increased microhardness throughout the deposit (197 HV) due to reduced heat input and faster cooling. Both image processing and density measurements confirmed the effectiveness of TS in controlling porosity, revealing a decrease in pore number and size with increasing TS. These findings emphasize that optimizing WAAM process parameters, particularly TS, is crucial for achieving minimal porosity and desired microhardness in ER70S-6 steel deposits, ultimately leading to high-quality, low-cost components.

**KEYWORDS:** Low Carbon Steel Alloy; Porosity; Mechanical Properties; Microstructure; Travel Speed (TS); Wire Arc Additive Manufacturing (WAAM).

## 1. INTRODUCTION

Wire Arc Additive Manufacturing (WAAM) has emerged as a powerful tool in industrial fabrication, offering rapid deposition rates for large-scale components compared to traditional additive manufacturing (AM) techniques. However, WAAM may require post-processing for high dimensional accuracy [1]. Leveraging simple equipment like robots or CNC systems, WAAM is particularly attractive for applications in aeronautics, automotive, defense, and other sectors due to its cost-effectiveness and reduced material waste compared to conventional machining [2].

The core principle of WAAM lies in Gas Metal Arc Welding (GMAW). This technology employs an electric arc generated between a consumable wire electrode and the base material. The resulting high temperatures, exceeding 10,000 Kelvin [3, 4], induce melting of the metal feedstock, forming a molten metal pool that serves as the building block for the desired component. However, precise control over this significant heat input is crucial for successful WAAM operation. Studies by Hauser et al. [5] have demonstrated the detrimental effects of exceeding the optimal temperature range. Their research showed that excessive temperatures during WAAM can lead to unwanted distortions and deviations from the intended design of the manufactured parts. This underscores the importance of meticulous process control in WAAM to guarantee the dimensional accuracy and structural integrity of the final component.

Steel is a compelling material choice for WAAM due to its inherent strength and ductility. Its ability to withstand substantial loads and accommodate thermal expansion during deposition helps prevent cracking within the structure [6]. Additionally, low-carbon steel like ER70S-6 exhibits excellent weldability due to minimal formation of brittle phases, ensuring smooth deposition and strong interlayer bonding. Furthermore, its cost-effectiveness compared to other WAAM materials makes ER70S-6 steel an attractive option for a wide range of applications.

Within WAAM technology, travel speed (TS) emerges as a critical factor influencing the final properties of deposited steel components. TS refers to the speed at which the deposition toolpath moves [7]. Optimizing TS is essential for achieving the desired microstructure and, consequently, the mechanical characteristics of the final WAAM-deposited steel component.

A major challenge in Additive Manufacturing (AM) is porosity. These voids within the material weaken components by reducing their overall density, significantly impacting tensile strength, the ability to resist pulling forces [8, 9]. In WAAM of steel, two main types of pores can form: hydrogen pores (smaller and uniformly distributed due to escaping hydrogen) and process pores (larger and irregular due to factors like improper welding parameters) [8, 10, 11].

The rapid solidification inherent to WAAM processes presents a significant challenge in achieving desirable microstructures within deposited steel components. The molten metal pool cools quickly as it deposits onto the base plate or previous layers, limiting the time available for grain nucleation and growth. This rapid solidification promotes the preferential growth of large, columnar grains along the heat flow direction, resulting in a coarse microstructure with inferior mechanical properties [12]. Additionally, the high heat input associated with WAAM can further exacerbate this issue by inducing grain coarsening.

This study aims to bridge a critical knowledge gap by investigating the influence of travel speed (TS), a crucial WAAM process parameter, on the porosity characteristics and resulting microstructure of ER70S-6 low carbon steel deposited using this technology. Elucidating this relationship holds significant scientific and engineering value [13]. While machine learning can streamline experimental efforts and reduce costs, a robust dataset encompassing a wide range of process parameters is essential for developing accurate predictive models [14-18].

Understanding how TS impacts porosity formation in ER70S-6 steel offers deeper insights into the solidification behavior of this specific alloy within the WAAM process. The low-carbon content of ER70S-6 steel is known to influence its material properties, particularly its solidification characteristics. This study will explore how this composition interacts with varying deposition speeds. By identifying the optimal TS range that minimizes porosity and promotes a finer microstructure, we can establish a foundation for process optimization specifically tailored for ER70S-6 steel. This knowledge will contribute to the scientific understanding of WAAM and its interaction with the solidification behavior of different materials.

From an engineering standpoint, investigating the TS-porosity relationship is paramount. Porosity is a well-established detriment to WAAM components, as it reduces density and consequently weakens mechanical performance. By establishing a clear correlation between TS and the formation of porosity in ER70S-6 steel, we can pave the way for the development of strategies to minimize this issue. This could involve optimizing shielding gas compositions to manage hydrogen entrapment, manipulating preheating temperatures to influence solidification rates, or implementing post-deposition treatments like hot isostatic pressing (HIP) to reduce porosity. Ultimately, this knowledge will empower engineers to design and manufacture more robust and reliable WAAM components using ER70S-6 steel.

This study investigates the relationship between TS, porosity, and microhardness in WAAM-deposited ER70S-6 steel. By examining this relationship, we aim to gain valuable insights into the AM process and its impact on both porosity and mechanical characteristics of WAAM-deposited components, leading to further advancements in producing low-cost and high quality ER70S-6 steel.

## 2. THE EXPERIMENTAL METHODS

### 2.1. MATERIALS

This study utilized ER70S-6 steel wire with a diameter of 0.8 mm as the feedstock material for WAAM deposition. This selection was driven by a combination of factors. ER70S-6 steel offers favorable mechanical properties, including good strength and weldability, making it suitable for WAAM applications. Additionally, it is a cost-effective choice for large-scale builds. The chosen wire diameter of 0.8 mm strikes a balance between printability, allowing for the creation of intricate features, and achieving a desired deposition rate to meet the study's objectives.

An AISI 1018 steel plate measuring 50 mm x 250 mm x 50 mm (thickness x length x width) served as the substrate for WAAM deposition. This material selection aimed to minimize residual stresses and potential warping during the process. AISI 1018 steel has a thermal expansion coefficient that closely matches that of ER70S-6 steel, reducing the risk of internal stresses and distortions that could compromise the integrity of the final component. To ensure proper adhesion between the deposited layers and enhance surface wettability, the substrate was meticulously cleaned with acetone and then underwent grit blasting.

Table 1 presents the chemical compositions of both the ER70S-6 wire and the ASTM 1045 steel plate for reference. Analyzing the elemental makeup of both materials provides valuable insights into potential interactions that may occur during the WAAM process and their influence on the final microstructure and properties of the deposited component.

### 2.2. WAAM PROCESS

A layer-by-layer WAAM technique was employed to investigate the relationship between travel speed and the mechanical properties of ER70S-6 steel deposits. To ensure optimal build quality and minimize thermal distortion, a controlled circulation system utilizing water and compressed air provided inter-layer cooling. Fig. 1(a) depicts a schematic of the experimental setup for thin-wall component deposition.

To precisely control heat input compared to conventional GMAW, a GTAW device, specifically a 350 A power supply (INV AC-DC PULSE TIG 350 A), served as the heat source for melting the ER70S-6 wire feedstock. For precise movement and deposition control, the GTAW torch was mounted on a three-axis CNC milling machine (Vcenter-102E).

Prior to WAAM deposition, the substrate plate surface was cleaned with acetone to remove any contaminants like oil or grease that could negatively impact adhesion and porosity formation. Extensive experimentation established optimal operational limits for the GTAW parameters, considering factors like arc stability, heat input, and deposition efficiency. Table 2 provides a comprehensive overview of the chosen process parameters and their corresponding levels. Notably, the investigation focused on three distinct TS values while maintaining other parameters constant. This approach isolates the specific effect of TS on porosity and mechanical properties, allowing for a controlled and systematic evaluation of its influence.

### 2.3. CHARACTERIZATION METHODS.

A multi-faceted approach was employed to assess the microstructure, microhardness, and porosity of the WAAM-deposited samples. First, the samples were sectioned as illustrated in Fig. 1(b). A meticulous polishing procedure followed, utilizing a sequence of abrasive sandpapers with progressively finer grits (400, 800, 1200, 2500, and 4000) to achieve a smooth, scratch-free surface for further analysis.

For microstructure characterization, the polished samples were etched with a 5% Nital solution to reveal grain boundaries and other features. A 3D laser microscope (LEXT OLS5100, Olympus, Japan) was then used to examine these etched surfaces. This advanced microscope provided high-resolution and depth-of-field images, enabling detailed observation of the microstructure across different layers and depths within the deposited material.

Microhardness measurements were conducted using a Vickers microhardness tester (Mitutoyo HM-210A series). Each indentation was applied with a standard dwell time of 15 seconds and a 500-gram load. To ensure representative measurements, samples for microhardness testing were precisely cut from the primary sample using a wire-cut electric discharge machine (EDM). This method minimizes thermal damage and ensures accurate geometry for reliable hardness determination.

### 2.4. POROSITY ANALYSIS:

In addition to the aforementioned techniques, the study also employed methods to quantify porosity. Digital images of the polished samples were analyzed using ImageJ software. This software excels at segmenting pores based on their grayscale intensity. By segmenting the pores, ImageJ enables the quantification of the total porosity percentage and the distribution of pore sizes within the samples.

Furthermore, Archimedes' principle was utilized to determine the densities of the WAAM-deposited samples. This established method involves measuring the mass of the sample in air and then submerged in water. By calculating the volume of water displaced and applying the known density of water, the actual density of the sample can be determined. This approach helps identify potential variations in density across the samples, which can be linked to differences in porosity.

*Table 1. Chemical composition of subtract and feedstock steel wire (in wt. %)*

| Elements | C | Mn | Si | P | S | Cu | Fe |
|---|---|---|---|---|---|---|---|
| Subtract (AISI 1018) | 0.17 | 0.5 | 0.22 | 0.02 | 0.03 | - | Bal. |
| Feedstock (ER70S-6) | 0.15 | 1.4 | 0.80 | 0.15 | 0.03 | 0.02 | Bal. |

*Table 2. WAAM deposition parameters*

| Parameter | Value |
|---|---|
| Type of welding current | DC |
| WFS | 5.5 m/min |
| Traveling speeds (TS) | 120, 150, 180 mm/min |
| Purity of argon shield gas | 99.99% |
| Flow rate of shield gas | 12 L/min |
| Current intensity | 300 A |
| Diameter of tungsten electrode | 2.4 mm |

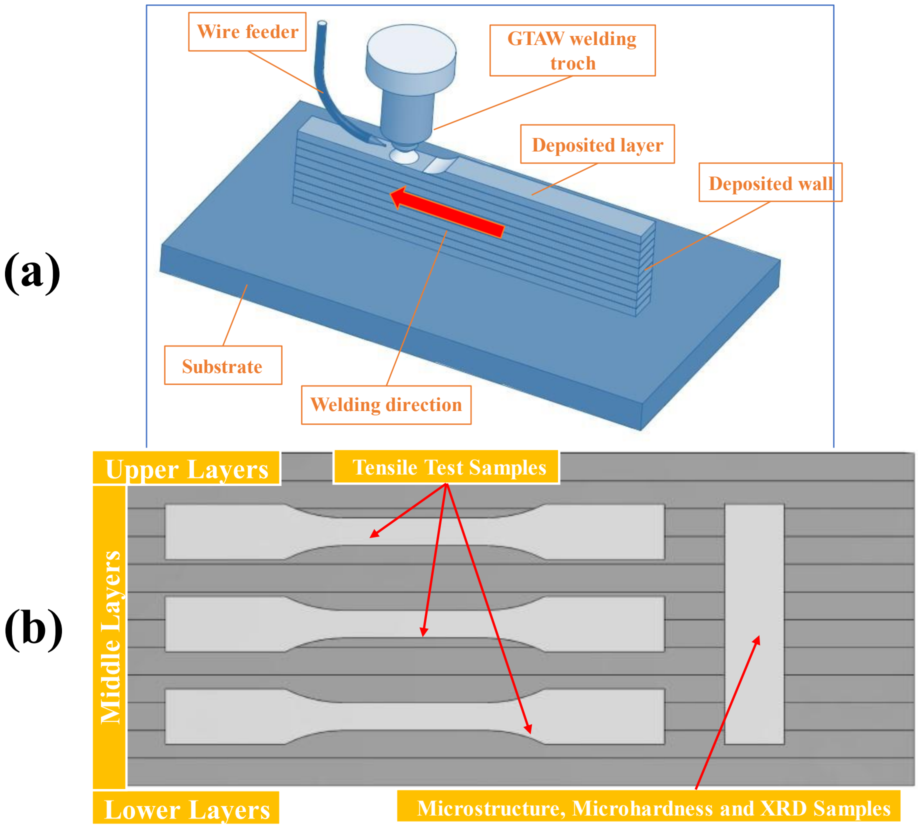


*Fig. 1. (a) Schematic of the WAAM system, and (b) Positions of microstructure and density samples.*

## 3. Results and Discussion

### 3.1. Challenges of Inadequate Parameters Selection in WAAM

The critical role of parameter selection in WAAM is underscored by the detrimental effects of inappropriate settings. Several key issues were encountered during the deposition process. The first challenge arose from using a slow travel speed of 150 mm/min in combination with a high DC current of 300 A (Fig. 2(a)). This resulted in a discontinuous weld bead, characterized by isolated or clustered droplets. This bead was entirely unsuitable for AM due to its uneven height and frequent interruptions. The culprit behind this issue was the excessive distance between the tungsten electrode and the substrate. This large gap hindered proper gas coverage of the molten metal pool, allowing oxygen to infiltrate and cause oxidation.

Another problem encountered was weld bead contamination, as seen in Fig. 2(b). Here, oxides were found adhering to the surface of the bead. This occurred due to an insufficient shielding gas flow rate of just 8 L/min. Shielding gas plays a vital role in protecting the molten metal from atmospheric contamination. With such a low flow rate, the gas coverage was inadequate, allowing oxide particles to freely attach to the deposited material. It's important to note that weld bead contamination can also arise from other factors, such as a complete lack of shielding gas, using an incorrect gas mixture, or having the gas blown away during the welding process.

A third issue observed was irregular layer formation, depicted in Fig. 2(c). These samples were deposited using a high TS (250 mm/min) coupled with a low wire feed rate of 3.5 m/min. This combination proved detrimental. The high TS meant the torch traveled too quickly, resulting in insufficient heat transfer between the deposited droplets and the underlying substrate. Additionally, the low wire feed rate limited the amount of material being fed into the melt pool. This combination starved the process of both heat and material, leading to an unstable arc with poor mechanical compression. Furthermore, the shielding gas flow rate also played a role. An improper flow rate can negatively influence the arc shape, causing erratic droplet transition and ultimately contributing to the observed irregular layer formation. The lack of proper gas shielding further exacerbated this problem by allowing significant oxidation to occur within the deposited layer. Rapid cooling of the droplets and inadequate preheating of the substrate could also worsen this issue, potentially leading to delamination (layer separation).

These examples serve as a stark reminder of the importance of meticulous parameter selection in WAAM. Finding the optimal balance between travel speed, wire feed rate, current, and shielding gas flow rate is crucial for achieving continuous, well-formed, and high-quality WAAM deposits.

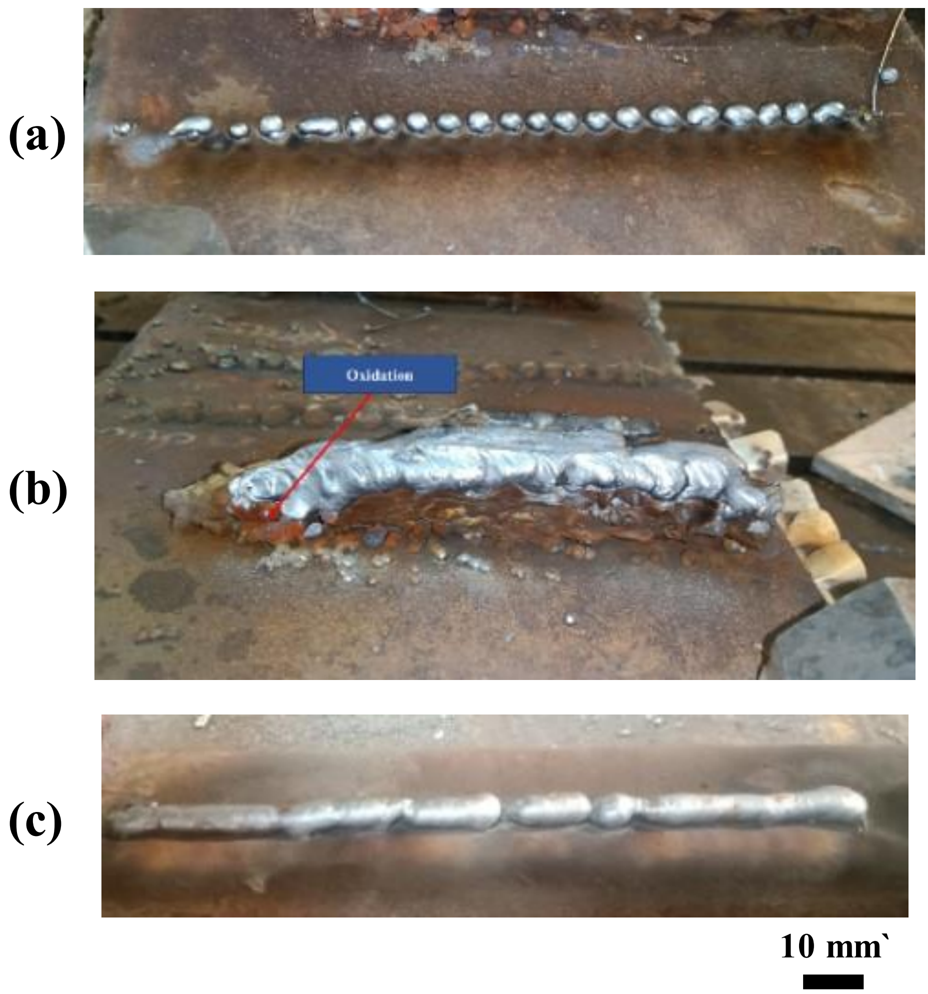


*Fig. 2. Typical images of (a) Discontinuous weld bead, (b) Contaminated weld bead, and (c) Irregular layer formation*

Deposition with a high WFS (5.5 m/min) and a low TS (60 mm/min) resulted in significant wall deformation, as illustrated in **Error! Reference source not found.** (a). This phenomenon can be attributed to the increased heat input caused by the imbalance between heat generation and heat dissipation. The high WFS continuously fed more material into the melt pool, while the slow TS limited the movement of the heat source (arc). This led to a localized concentration of heat, causing the molten metal to flow laterally instead of building up vertically, resulting in the observed wall deformation.

The surface morphology and dimensional accuracy of WAAM components are highly sensitive to the chosen process parameters, particularly TS, WFS, and current. Systematic experimentation revealed that increasing TS or decreasing WFS generally reduced the height and width of the deposited material. This can be explained by the reduced heat input associated with faster travel speeds or lower wire feed rates. Less heat input results in a smaller molten pool and consequently a lower deposited layer profile.

Operating with a low TS and a high WFS promoted the formation of multiple weld ripples (Fig. 3(a)). The extended dwell time of the molten metal droplets due to the slow travel speed allowed them to grow larger before solidification, leading to the formation of coarser and wider ripples on the deposited surface. Conversely, reducing the current resulted in a decrease in both heat input and weld thickness. This was manifested as narrower walls at the bottom of the deposited component due to the lower overall material addition. However, the top section exhibited distortion likely caused by residual heat from previous layers due to the reduced heat dissipation at that location.

Fig. 3(b) presents a sample fabricated with optimized process parameters, highlighting the significant improvement in geometric control and surface quality achievable through proper parameter selection.


*Fig. 3. Typical images of (a) Excessive melting of metal due to high heat concentration, (b) Full appearance of the deposited sample.*

## 3.2. Microstructure and Porosity Analysis

### 3.2.1. MICROSTRUCTURE AND COOLING RATES

There is a well-established correlation between microstructure and cooling rates in WAAM [19]. The observed primary phases of pearlite and ferrite are consistent with previous findings [20], emphasizing the impact of heat input per unit length on solidification and subsequent phase transformation. However, our investigation goes beyond these primary phases, identifying the presence of additional microconstituents such as acicular ferrite, bainite, Widmanstatten ferrite, and transformed martensite [20, 21]. This complex microstructure likely arises from the dynamic interplay between cooling rates, variations in heat input within the deposited bead, and the interaction between subsequent layers during deposition.

### 3.2.2. POROSITY AND ITS ORIGINS

The observed porosity within the microstructure (Fig. 4) aligns with the known challenges associated with hydrogen entrapment during arc welding of steel alloys. These pores can significantly compromise the mechanical properties, corrosion resistance, and fatigue life of the material. As previous studies have shown, factors like repeated thermal cycles, improper parameter selection, and turbulent welding conditions can exacerbate pore formation.

### 3.2.3. TRAVEL SPEED AND POROSITY CONTROL

The observation shows increased pore formation at a lower TS of 120 mm/min compared to 180 mm/min supports the established relationship between heat input and porosity [22]. Eq.1 accurately describes this dependency, highlighting how TS directly influences heat input and consequently, pore formation. This finding aligns with previous research demonstrating the detrimental effect of lower TS on pore characteristics and density in WAAM-deposited materials [23, 24].

The significantly reduced pore occurrence at a TS of 180 mm/min suggests this parameter plays a crucial role in controlling microstructure and porosity in WAAM-deposited ER70S-6 steel. This aligns with prior studies emphasizing the importance of TS optimization for achieving desired microstructure and mechanical properties in WAAM [25, 26]. These results contribute to this growing body of knowledge by highlighting the specific impact of TS on porosity within the context of ER70S-6 steel, underlining its critical role in ensuring optimal component quality.

$$\mathrm{HI} = \frac{V \times I}{TS} \times \eta \times 0.06 \qquad (1)$$

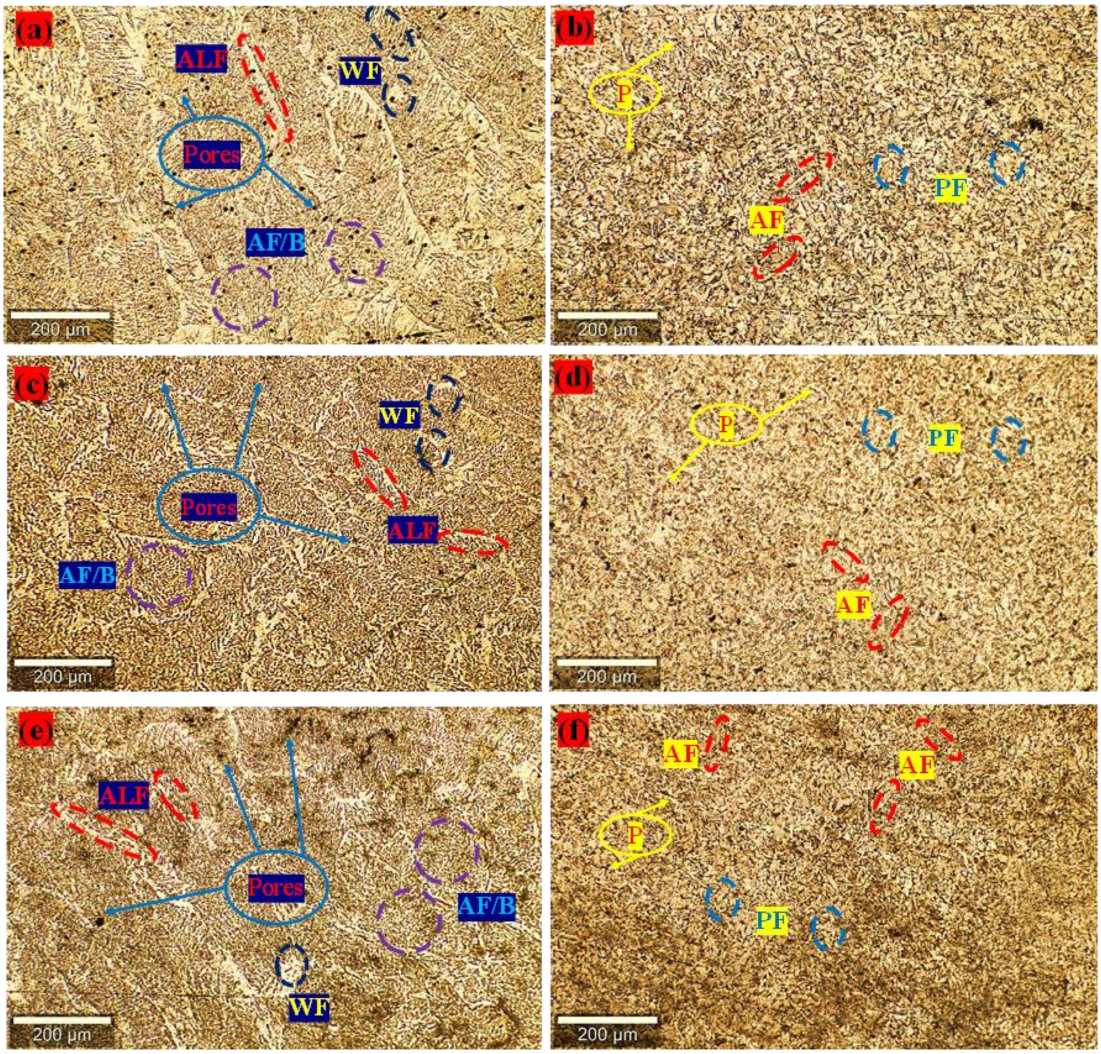


*Fig. 4. Microstructure analysis of the top-layer region (a, c, and e) and middle-layer region (b, d, and f) in the deposited samples at varying TS using an optical microscopy: (a), (b) at 120 mm/min, (c), (d) at 150 mm/min, and (e), (f) at 180 mm/min.*

## 3.3. MICROHARDNESS EVALUATIONS

The observed variations in microhardness across different regions of the WAAM-deposited ER70S-6 steel highlight the interplay between heat transfer, microstructure development, and resulting mechanical properties. Travel speed is identified as a key factor influencing these relationships.

### 3.3.1. MICROHARDNESS VARIATIONS

The observed microhardness variations across different regions and TS emphasize the complex interaction between heat transfer, microstructure, and ultimately, the mechanical properties of WAAM-deposited ER70S-6 steel. A consistent trend emerged, with both the bottom and top regions exhibiting higher microhardness compared to the middle region (e.g., 216 vs. 186 HV at 150 mm/min). This aligns with established principles that link thermal history to the resulting microstructure and properties [27].

The higher microhardness in the bottom and top regions can be attributed to their contrasting thermal experiences. Bottom layers, in direct contact with the substrate, act as a heat sink, facilitating faster heat transfer and consequently, rapid cooling. This rapid cooling promotes the development of a finer microstructure, which in turn leads to greater microhardness [28]. Similarly, top layers often experience accelerated cooling due to water cooling strategies, leading to a similar refinement of the microstructure and enhanced hardness. This finding is consistent with previous research on WAAM-deposited materials, demonstrating the influence of cooling rate on both microstructure and hardness [29, 30].

### 3.3.2. TRAVEL SPEED AND MICROHARDNESS

The observed trend of increasing microhardness with increasing TS (178 HV at 120 mm/min vs. 197 HV at 180 mm/min) aligns with the established relationship between TS, heat input, and cooling rate (Fig. 5). Eq.1 accurately describes this dependency, highlighting that a reduction in heat input due to higher TS promotes faster cooling [30]. This rapid cooling, as demonstrated in **Error! Reference source not found.** by the reduced layer thickness at higher TS, facilitates the development of a finer microstructure, contributing to the observed increase in microhardness [31].

### 3.3.3. MICROHARDNESS AND POROSITY

As shown in Fig. 6, the sample processed at a lower TS (120 mm/min) exhibited a higher presence of pores compared to samples processed at higher TS. This aligns with the established relationship between TS, heat input, and porosity [32]. Lower TS corresponds to higher heat input, which can exacerbate hydrogen entrapment and pore formation. The reduction in pore size and quantity observed at 150 mm/min suggests a potential balance between heat input and cooling rate, mitigating excessive pore formation. However, the complete absence of pores at the highest TS (180 mm/min) indicates that further optimization might be needed to ensure consistent porosity control across the entire deposit. This finding aligns with previous research highlighting the complex interplay between process parameters and porosity in WAAM [26, 33]

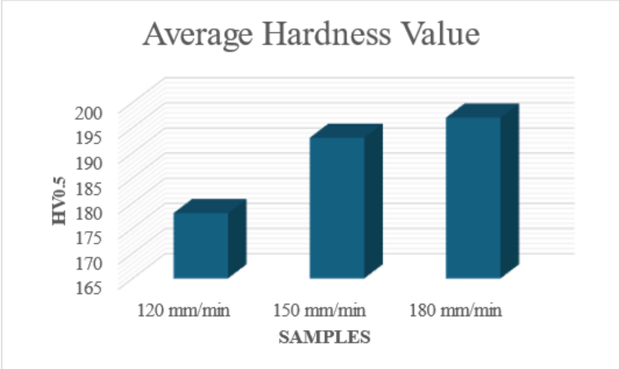


*Fig. 5. Average hardness values of the deposited samples*

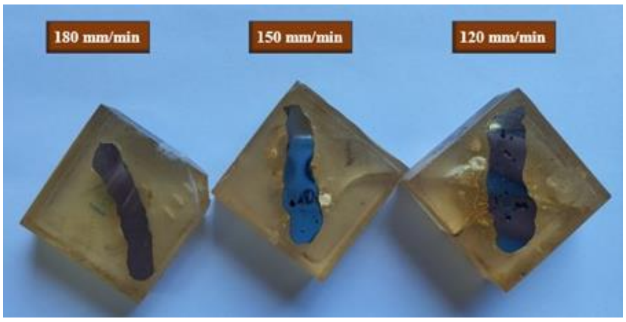


*Fig. 6. Typical images of the polished samples for microstructure analysis.*

## 3.4. POROSITY QUANTIFICATION

The assessment of porosity within WAAM-deposited ER70S-6 steel employed two complementary techniques: image processing and density measurement. ImageJ software facilitates the visualization of pores, revealing a clear increase in their occurrence at lower travel speeds (TS) (Fig. 7).

Table 3 quantifies this observation, presenting the percentage of pore area relative to the entire analyzed surface. The data shows a decreasing trend in porosity with increasing TS: 3.607% - 9.347% at 120 mm/min, decreasing to 2.136% - 6.295% at 150 mm/min, and further down to 1.234%

- 2.827% at 180 mm/min.

A volumetric approach based on Archimedes' principle was employed to determine the density of each sample. The measured densities are presented in Table 3: 7108.875 kg/m³ (120 mm/min), 6167.207 kg/m³ (150 mm/min), and 7609.023 kg/m³ (180 mm/min). By comparing these values to the standard density of 7800 kg/m³ for conventionally produced ER70S-6 alloys, an estimation of porosity was obtained. The calculated porosity values for samples deposited at 120 mm/min, 150 mm/min, and 180 mm/min were 15.58%, 5.68%, and 2.04%, respectively.

Both image analysis and density measurement techniques consistently reveal a direct relationship between TS and porosity. As observed in Fig. 7, and confirmed by the data in Table 3the number and size of pores decrease significantly with increasing TS. This trend aligns with previous research demonstrating that lower TS leads to higher heat input, promoting hydrogen entrapment and increased pore formation [34, 35].

These observations align with previous studies highlighting the influence of travel speed on porosity in additive manufacturing processes. For instance, H.M. et al. [36] reported a 23% decrease in pore volume in WAAM-deposited stainless steel with increased TS, attributing this to faster cooling and reduced hydrogen solubility. Similarly, Wang et al. [37] observed a significant reduction in porosity in additively manufactured Ti-6Al-4V components at higher TS due to rapid solidification and limited pore growth. The present study extends these findings to ER70S-6 steel, demonstrating the general applicability of this relationship across different material systems.

The combined application of image processing and density measurement provides a comprehensive assessment of porosity in WAAM-deposited ER70S-6 steel. The observed decrease in porosity with increasing TS aligns with established knowledge about the influence of TS on heat input and hydrogen entrapment. These findings highlight the critical role of optimizing TS as a parameter for controlling porosity and achieving high-quality WAAM components.

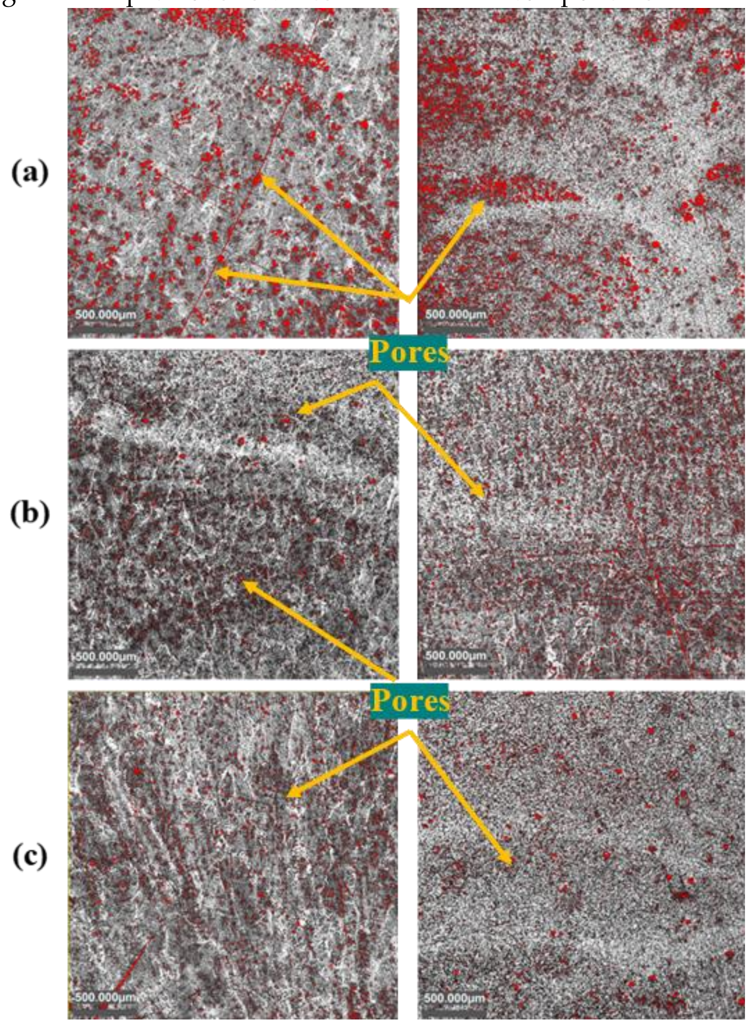


*Fig. 7. Optical microscopy analysis (5X Lens) of deposited samples at different travel speeds (a) 120 mm/min, (b) 150 mm/min, (c) 180 mm/min*

*Table 3. The density of WAAM samples based on the Archimedes' principle.*

| Sample | Sample Weight (gram) | Water Weight (gram) | Sample Weight + Water Weight | Sample Volume ($mm^3$) | Density ($kg/m^3$) |
|---|---|---|---|---|---|
| **120 mm/min** | 1.8021 | 75.7818 | 76.0353 | 253.5 | 7108.875 |
| **150 mm/min** | 1.7114 | 75.7216 | 75.9991 | 277.5 | 6167.207 |
| **180 mm/min** | 2.1252 | 75.6827 | 75.962 | 279.3 | 7609.023 |

## 4. CONCLUSIONS

This study explored the influence of travel speed (TS) on porosity and microhardness in WAAM-deposited ER70S-6 steel. A clear correlation emerged, with lower TS leading to significantly higher porosity. This can be attributed to the increased heat input at lower TS, promoting hydrogen entrapment and pore formation. Samples deposited at 120 mm/min exhibited a substantially higher pore area percentage (3.61%-9.35%) compared to those at 180 mm/min (1.23%-2.83%), signifying a remarkable 73% enhancement in porosity reduction at the higher speed. This aligns perfectly with established knowledge, highlighting the critical role of TS optimization for effective porosity control in WAAM. The relationship between TS and microhardness was more intricate. Faster cooling rates in bottom and top regions due to substrate contact or water cooling resulted in higher microhardness compared to the middle region. However, increasing TS demonstrably promoted a favorable microstructure across the entire deposit, leading to a notable increase in microhardness (up to 11% at 180 mm/min compared to 178 HV at 120 mm/min). This finding underscores the complex interplay between heat transfer, microstructure development, and the resulting mechanical properties in WAAM deposits. To comprehensively assess porosity, the study employed a combined approach utilizing both image processing and density measurement techniques. Both methods consistently revealed a significant decrease in the number and size of pores with increasing TS. This synergy emphasizes the importance of employing complementary methods for a more thorough evaluation of porosity in WAAM-deposited materials. The findings underline TS as a critical parameter for optimizing WAAM. By implementing an optimal TS, researchers and engineers can achieve high-quality WAAM components with minimized porosity and enhanced mechanical properties, paving the way for the fabrication of stronger and less porous functional parts.

## 5. FUTURE WORK

Future work will focus on optimizing WAAM through machine learning-based predictive modeling and metaheuristic optimization to achieve real-time process control and improved part quality.


### ACKNOWLEDGMENT

The authors would like to express their sincere gratitude to the Faculty of Engineering at Kafrelsheikh University for their support in providing access to facilities and laboratories for this research. Furthermore, they wish to extend their heartfelt appreciation to the anonymous reviewers for their valuable contributions and insightful comments, which greatly improved the quality of this work.

### DECLARATION OF COMPETING INTEREST

The authors declare that they have no known competing financial interests or personal relationships that could have appeared to influence the work reported in this paper.


## REFERENCES


[1] Z. Wang, Y. Zhang, A Review of Aluminum Alloy Fabricated by Different Processes of Wire Arc Additive Manufacturing, Materials Science 27(1) (2021) 18-26.

[2] T.A. Rodrigues, V. Duarte, R.M. Miranda, T.G. Santos, J.P. Oliveira, Current Status and Perspectives on Wire and Arc Additive Manufacturing (WAAM), 12(7) (2019) 1121.

[3] S. Zielińska, K. Musioł, K. Dzierżęga, S. Pellerin, F. Valensi, C. de Izarra, F. Briand, Investigations of GMAW plasma by optical emission spectroscopy, Plasma Sources Science and Technology 16(4) (2007) 832.

[4] M. Moheyeldin Mahmoud, Using of Polyethylene Terephthalate (PET) Panels in Product Design: A Safe Disposal for Plastic Waste, Journal of Contemporary Technology and Applied Engineering 3(1) (2024) 1-10.

[5] T. Hauser, A.D. Silva, R.T. Reisch, J. Volpp, T. Kamps, A.F.H. Kaplan, Fluctuation effects in Wire Arc Additive Manufacturing of aluminium analysed by high-speed imaging, Journal of Manufacturing Processes 56 (2020) 1088-1098.

[6] C.N. Agusiegbe, D. Morton, E. Moore, High-Carbon Steel in Additive Manufacturing, (2022).

[7] H.T. Serindağ, G. Çam, Characterizations of Microstructure and Properties of Dissimilar AISI 316L/9Ni Low-Alloy Cryogenic Steel Joints Fabricated by Gas Tungsten Arc Welding, Journal

of Materials Engineering and Performance 32(15) (2023) 7039-7049.

[8] J. Gu, J. Ding, S.W. Williams, H. Gu, P. Ma, Y. Zhai, The effect of inter-layer cold working and post-deposition heat treatment on porosity in additively manufactured aluminum alloys, Journal of Materials Processing Technology 230 (2016) 26-34.

[9] M.H.G. Alsaadawy, M.M. dewidar, A.H. Said, I.M. Sultan, T.A. Shehabeldeen, Investigation of Effect of Laser Cutting Parameters on Microhardness and Average Kerf Width of Ti-6Al-4V Alloy, Journal of Contemporary Technology and Applied Engineering 2(2) (2023) 53-68.

[10] M. Anis, K. Derekar, J. Lawrence, G. Melton, A. Addison, X. Zhang, L. Xu, B. Munir, Influence of Interpass Temperature on Wire Arc Additive Manufacturing (WAAM) of Aluminium Alloy Components, MATEC Web of Conferences 269 (2019).

[11] C. Chen, X. Wei, Y. Zhao, K. Yan, Z. Jia, Y. He, Effects of helium gas flow rate on arc shape, molten pool behavior and penetration in aluminum alloy DCEN TIG welding, Journal of Materials Processing Technology 255 (2018) 696-702.

[12] C.R. Cunningham, J.M. Flynn, A. Shokrani, V. Dhokia, S.T. Newman, Invited review article: Strategies and processes for high quality wire arc additive manufacturing, Additive Manufacturing 22 (2018) 672-686.

[13] V.T. Le, A preliminary study on gas metal arc welding-based additive manufacturing of metal parts, Science and Technology Development Journal 23 (2019).

[14] A.H. Elsheikh, Applications of machine learning in friction stir welding: Prediction of joint properties, real-time control and tool failure diagnosis, Engineering Applications of Artificial Intelligence 121 (2023) 105961.

[15] M. Abd Elaziz, A.H. Elsheikh, D. Oliva, L. Abualigah, S. Lu, A.A. Ewees, Advanced Metaheuristic Techniques for Mechanical Design Problems: Review, Archives of Computational Methods in Engineering 29(1) (2022) 695-716.

[16] M.A. Elaziz, F.A. Essa, H.A. Khalil, M.S. El-Sebaey, M. Khedr, A. Elsheikh, Productivity prediction of a spherical distiller using a machine learning model and triangulation topology aggregation optimizer, Desalination 585 (2024) 117744.

[17] S.P. Parida, P.C. Jena, S.R. Das, A. Basem, A.K. Khatua, A.H. Elsheikh, Transverse vibration of laminated-composite-plates with fillers under moving mass rested on elastic foundation using higher order shear deformation theory, Proceedings of the Institution of Mechanical Engineers, Part C: Journal of Mechanical Engineering Science (2024) 09544062241256589.

[18] A.H. Elsheikh, M. Abd Elaziz, B. Ramesh, M. Egiza, M.A.A. Al-qaness, Modeling of drilling process of GFRP composite using a hybrid random vector functional link network/parasitism-predation algorithm, Journal of Materials Research and Technology 14 (2021) 298-311.

[19] A.S. Yildiz, K. Davut, B. Koc, O. Yilmaz, Wire arc additive manufacturing of high-strength low alloy steels: study of process parameters and their influence on the bead geometry and mechanical characteristics, The International Journal of Advanced Manufacturing Technology 108(11) (2020) 3391-3404.

[20] P. Dirisu, S. Ganguly, A. Mehmanparast, F. Martina, S. Williams, Analysis of fracture toughness properties of wire + arc additive manufactured high strength low alloy structural steel components, Materials Science and Engineering: A 765 (2019) 138285.

[21] M. Ghaffari, A. Vahedi Nemani, M. Rafieazad, A. Nasiri, Effect of Solidification Defects and HAZ Softening on the Anisotropic Mechanical Properties of a Wire Arc Additive-Manufactured Low-Carbon Low-Alloy Steel Part, Jom 71(11) (2019) 4215-4224.

[22] D. Gu, W. Meiners, K. Wissenbach, R. Poprawe, Laser additive manufacturing of metallic components: Materials, processes and mechanisms, International Materials Reviews 57 (2012) 133-164.

[23] Y. Khandelwal, R. Kumar, K. Verma, A. Mandal, A Study of Microstructure and Mechanical Properties of Wire Arc Additive Manufactured Component with ER70S6 Alloy Wire Using CMT Process, 2021, pp. 133-146.

[24] R. Kapoor, A. Sarkar, A.N. Behera, S. Sunil, Multi-axial forging of Nb-1wt.%Zr: Effect of annealing on microstructure and mechanical properties, Materials Science and Engineering: A 772 (2020) 138805.

[25] Y. Zhou, X. Lin, N. Kang, W. Huang, J. Wang, W. Zhennan, Influence of travel speed on microstructure and mechanical properties of wire + arc additively manufactured 2219 aluminum alloy, Journal of Materials Science and Technology -Shenyang- (2019).

[26] A. Astarita, G. Campatelli, P. Corigliano, G. Epasto, F. Montevecchi, F. Scherillo, G. Venturini, Microstructure and mechanical properties of

specimens produced using the wire-arc additive manufacturing process, Proceedings of the Institution of Mechanical Engineers, Part C: Journal of Mechanical Engineering Science 235(10) (2019) 1788-1798.

[27] B. Song, S. Dong, B. Zhang, H. Liao, C. Coddet, Effects of processing parameters on microstructure and mechanical property of selective laser melted Ti6Al4V, Materials & Design 35 (2012) 120–125.

[28] W. Zhai, N. Wu, W. Zhou, Effect of Interpass Temperature on Wire Arc Additive Manufacturing Using High-Strength Metal-Cored Wire, Metals, 2022.

[29] Y. Khebreh Farshchi, F. Khodabakhshi, M. Mohri, H. Shirazi, M. Nili-Ahmadabadi, Microstructural engineering in carbon steel walls printed by directed energy deposition to enhance mechanical properties through heat-input control, Journal of Materials Research and Technology 28 (2024) 490-499.

[30] S. Zhang, Y. Zhang, J. Qi, Z. Zou, Y. Qian, Effect of Heat Treatment on the Microstructure and Mechanical Properties of Additive Manufactured Ti-6.5Al-2Zr-1Mo-1V Alloy, Materials, 2023.

[31] M. Waqas, D. He, Y. Liu, S. Riaz, F. Afzal, Effect of Heat Treatment on Microstructure and Mechanical Properties of Ti6Al4V Alloy Fabricated by Selective Laser Melting, Journal of Materials Engineering and Performance 32 (2022) 1-15.

[32] B.P. Nagasai, S. Malarvizhi, V. Balasubramanian, Mechanical properties of wire arc additive manufactured carbon steel cylindrical component made by gas metal arc welding process, 30(1) (2021) 188-198.

[33] Q. Fang, L. Zhao, C. Chen, Y. Zhu, Y. Peng, F. Yin, Effect of heat input on microstructural and mechanical properties of high strength low alloy steel block parts fabricated by wire arc additive manufacturing, Materials Today Communications 34 (2023) 105146.

[34] T. Hauser, R.T. Reisch, P.P. Breese, B.S. Lutz, M. Pantano, Y. Nalam, K. Bela, T. Kamps, J. Volpp, A.F.H. Kaplan, Porosity in wire arc additive manufacturing of aluminium alloys, Additive Manufacturing 41 (2021) 101993.

[35] M. Arana, E. Ukar, I. Rodriguez, A. Iturrioz, P. Alvarez, Strategies to Reduce Porosity in Al-Mg WAAM Parts and Their Impact on Mechanical Properties, Metals 11(3) (2021).

[36] V. H M, R. Rao, M. Maiya, P. Kumar, N. Gupta, K. Saxena, V. Vijayan, Effects of arc current and travel speed on the processing of stainless steel via wire arc additive manufacturing (WAAM) process, J. Adhes. Sci. Technol. (2023) 1-18.

[37] F. Wang, S. Williams, P. Colegrove, A.A. Antonysamy, Microstructure and Mechanical Properties of Wire and Arc Additive Manufactured Ti-6Al-4V, Metallurgical and Materials Transactions A 44(2) (2012) 968-977.